

Band structures and optical properties of two transition-metal carbides—TiC and ZrC[†]

J. F. Alward and C. Y. Fong

Department of Physics, University of California, Davis, California 95616

M. El-Batanouny* and F. Wooten

Department of Applied Science, University of California, Davis, California 95616

(Received 2 January 1975)

The optical reflectivities of face-centered-cubic TiC and ZrC have been measured in the range $1.0 \leq \hbar\omega \leq 8.0$ eV. In addition, the electronic-energy-band structures for these compounds have been calculated using a modified empirical-pseudopotential method, and the structures in the reflectivities derived from these band structures show approximate one-to-one correspondence to the structures in the data, with agreement to the order of 0.2 eV. Prominent structures in the measured reflectivities of both compounds are identified.

I. INTRODUCTION

Their extremely high melting points, exceptional hardness, and high superconducting temperatures have made refractory metal carbides among the most extensively investigated transition-metal compounds.¹ Owing both to its ready availability in the form of good, single crystals, and to the fact that its *d* states are the easiest to treat theoretically, much of the attention in the past has focused on TiC. Still, many features of bonding in this carbide have not been satisfactorily explained, in part because of the scarcity of good optical measurements needed to verify its calculated electronic band structure. Many contradictory theories have attempted to resolve the relative importance of ionic, covalent, and metallic bonding in TiC. A few theories emphasize strong metal-nonmetal bonds,²⁻⁴ wherein the *d*-like electrons of the metal atom form strong covalent bonds with the *sp* electrons of the carbon atom; the most recent studies stress simultaneous contributions of metallic, covalent, and ionic bonding.⁵⁻⁹ A problem central to all of these theories is the determination of the relative position and degree of admixture of the carbon *2s* and *2p* levels with the *3d* and *4s* states of titanium. To answer this, we have begun a systematic study of the optical properties of TiC and a closely related compound, ZrC, in order to obtain band structures which adequately explain the optical data which we have obtained. A detailed analysis of the bonding properties of these compounds will be made soon and the results will be presented in a future publication.

Until now, the only optical measurements on ZrC have been on a sample of relatively low stoichiometry (see footnote 11 in Ref. 6), and the most recent available optical information for TiC has been a reflectivity measurement which showed little detailed structure below 3 eV.⁶ We have recently completed detailed measurements of the reflectivities of face-centered-cubic TiC and ZrC in the

range $1.0 \leq \hbar\omega \leq 8.0$ eV. In addition, we have calculated their electronic energy band structures using the usual empirical-pseudopotential method (EPM),¹⁰ as modified by Fong and Cohen,^{11,12} and the theoretical reflectivity spectra derived from these band structures show satisfactory agreement with the data. This agreement between measurement and calculation gives some validity to the band structures of both TiC and ZrC, and not only helps resolve a TiC band-ordering controversy engendered by previous conflicting results involving the augmented plane wave,⁸ self-consistent augmented plane wave,⁹ and the tight-binding schemes,^{2,6} but also clears the way for a more detailed future examination of the unique bonding and superconducting properties of these compounds.

In Sec. II we discuss briefly the details of the sample preparation and point out the unique features of the experimental apparatus. In Sec. III we outline specifics of the modified EPM approach to the present band-structure calculations. Our theory and data for TiC are compared with related previous results in Sec. IV; in Sec. V we present the results for ZrC, and finally, in Sec. VI we give our conclusions and summary of the results for both compounds.

II. EXPERIMENT

In this section we shall discuss some operational details of the reflectometer, and then outline the methods of sample preparation and measurement of the reflectivity.

A. Reflectometer

The apparatus used in the present measurements are the same as those used by Irani *et al.*¹³ A schematic diagram given in Fig. 1 shows the main features of the system. The reflectometer¹³ (not shown) is based on single beam normal incidence reflectance measurements. The use of the same single-reflecting mirror for both incident and reflected beams eliminates many of the inherent weak-

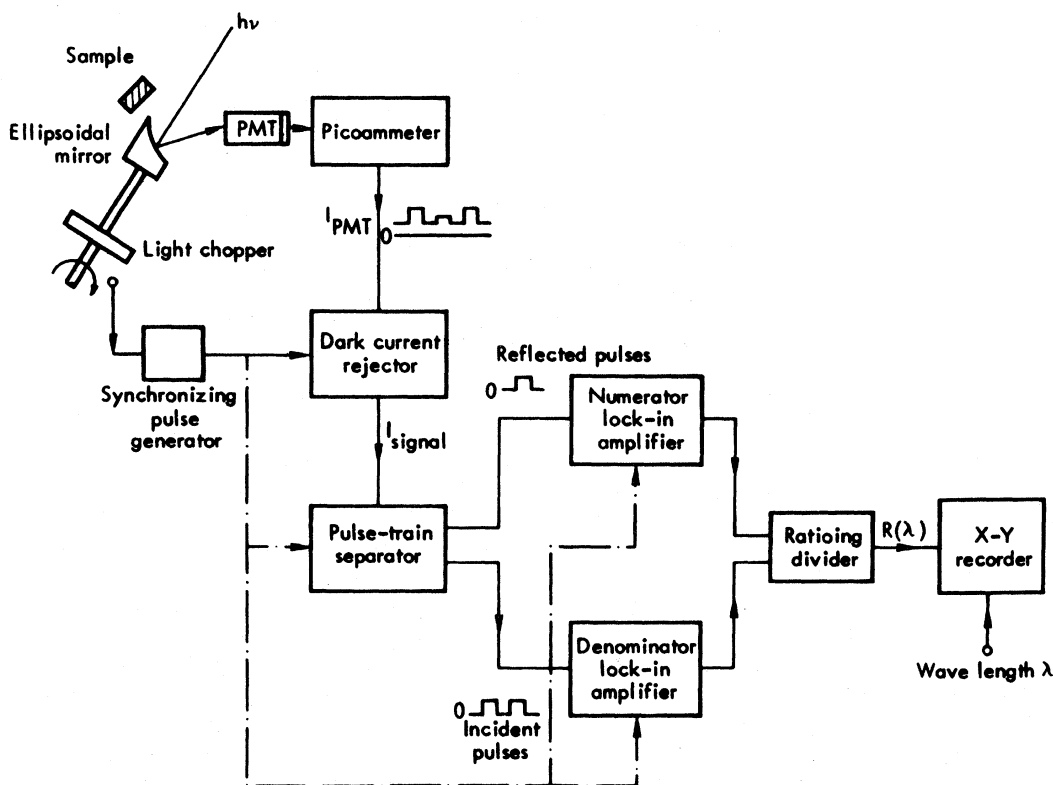


FIG. 1. Block diagram of reflectance-ratio measurement system.

nesses found in double-beam systems, in particular, the inevitable spectral mismatch of optical components used in the two beams of a double-beam instrument. Moreover, problems arising from the point-by-point measurement method, in particular the long-term instability of dc electronics and intensity variations of light sources that limit the accuracy, are avoided by using continuous scanning and ac chopping techniques. This is implemented by a rotating mirror that directs the incident and reflected beams consecutively onto the light detector. An ellipsoidal geometry is adopted in the mirror design to control the projection of the incident and reflected beams on the same spot of the detector, thus avoiding the problem of spectral-response variations across the tube. The detected signal is in the form of a series of current pulses from the photomultiplier which are subsequently separated electronically into incident and reflected trains, respectively. This is followed by electronic averaging and ratio taking. The desired spectral-reflectance curve is traced by recording the ratio as the wavelength is automatically scanned. The implementation of the above features provide a very good resolution as has been demonstrated in measurements on pure silver and silver-aluminum alloys.¹⁴

B. Sample preparation

Wafers of $\text{TiC}_{0.999}$ and $\text{ZrC}_{1.004}$ were hot-pressed at 2100–2200 °C for three h at 3000 psi. These samples were then polished with diamond paste down to $\frac{1}{4}$ - μm grit.

We performed a metallographic examination of the samples and observed fine-grain structure with no second phase present. This is to be expected on the basis of an examination of the phase diagrams for these carbides. Some carbon from the carbon die is expected to contaminate the outer regions of the samples. However, it was only necessary to grind off the surface regions to remove the excess carbon.

The surfaces were cleaned with trichloroethane and then rinsed with freon TF. The samples were then mounted in the reflectometer, which was then evacuated to a pressure of about 10^{-6} Torr, and baked at a temperature of 80 °C for two days (the low bakeout temperature was necessary to protect the photomultiplier tube) after which a base pressure of 10^{-9} Torr was reached. To ensure removal of any residual contaminants on the surface, argon ion-bombardment technique were employed. Argon gas was leaked into the chamber to a pressure of about 200 mTorr, and a discharge was then main-

tained between an anode and the sample as a cathode for 5 min. After recovery to the base pressure, the sample was heated for about 12 h at 200 °C to ensure outgasing of any argon ions absorbed on the sample surface and to provide some annealing of the sample.

C. Reflectance measurements

Measurements were made in the range $1 \leq \hbar\omega \leq 8$ eV. A Bausch and Lomb monochrometer was used for measurements in the range $1 \leq \hbar\omega \leq 5$ eV, providing a resolution of 0.01 eV or better, and deuterium and tungsten lamps were used in the ranges $3 \leq \hbar\omega \leq 5$ eV and $1 \leq \hbar\omega \leq 3.5$ eV, respectively. A McPherson model 225 monochrometer with a hydrogen-discharge lamp was used in the range $4 < \hbar\omega < 8$ eV, with a resolution of 0.08 eV or better. Appropriate filters were used to eliminate the second-order light. The absolute value of the reflectivity was determined by a pulse-height measurement at a particular wavelength ($\sim 10\,300$ Å) where the signal was sufficiently strong to provide a signal-to-noise ratio better than 20 dB. Reflectance curves obtained from different spectral regions were joined in the over-lapping regions by a least-squares fit and then the resulting curve was normalized to the available absolute value.

III. THEORY

For each carbide, the present work involves the determination of a band structure and reflectivity spectrum consistent with the experimental data. In the sections below we discuss our methods of calculation.

A. Calculation of electronic band structures

A complete explanation of the modified empirical pseudopotential method is given elsewhere,^{11,12} so we shall mention only the most relevant details here.

Our pseudopotential Hamiltonian

$$H = T + V_L(\vec{r}) + V_{NL}(\vec{r}) \quad (1)$$

consists of three parts: (i) the kinetic energy T ; (ii) the local pseudopotential $V_L(\vec{r})$; and (iii) a non-local part $V_{NL}(\vec{r})$, which is used to represent the strong attractive d potential which is over cancelled by the assumption of the weak local pseudopotential. The usual Fourier expansion of the weak local pseudopotential

$$V_L(\vec{r}) = \sum_{\vec{G}} V(\vec{G}) e^{-i\vec{G}\cdot\vec{r}} \quad (2)$$

is truncated at $|\vec{G}|^2 = 12$, where \vec{G} is a reciprocal-lattice vector in units of $2\pi/a$, a is the lattice constant, and $V(\vec{G})$ are the pseudopotential form factors. Previous EPM calculations on NbC,¹⁵ and on NbN,¹² have employed a nonlocal p -wave pseudopo-

tential, but we have found that a band structure consistent with the data may be found for each compound without using this potential. Our d -wave pseudopotential, though, is of the same form as that used in Ref. 12,

$$V_{NL}(\vec{r}) = \sum_j P_d^\dagger V_d(|\vec{r} - \vec{R}_j|) P_d, \quad (3)$$

where \vec{R}_j is a lattice vector, and P_d is an operator which projects out the $l=2$ (d -like) component of the wave functions. The d potential is taken to be a constant within a sphere, and zero outside,

$$V_d(|\vec{r} - \vec{R}_j|) = \begin{cases} A_d & \text{for } |\vec{r} - \vec{R}_j| \leq R_d \\ 0 & \text{otherwise} \end{cases}, \quad (4)$$

where the depth and radius of the spherical well are treated as adjustable parameters.

To facilitate d -band energy convergence, a damping factor is applied to the matrix elements of V_{NL} to obtain the modified matrix elements

$$e^{-\eta} \langle \vec{k} + \vec{G} | V_{NL} | \vec{k} + \vec{G}' \rangle e^{-\eta'}, \quad (5)$$

where

$$\eta = \alpha [(|\vec{k} + \vec{G}| - \kappa) / 2k_F]^p;$$

α and κ are treated as parameters, and k_F is the Fermi momentum of the metal atom.

We start the TiC calculation with a set of form factors obtained by scaling the potentials used in a previous calculation of NbN,¹² in order to account for the difference in the lattice constants. These potentials are then adjusted until the general shape and position of structure in the calculated reflectivity agrees reasonably well with the experiment. The band structures are calculated on a mesh of 46 points in $\frac{1}{48}$ of the Brillouin zone.

B. Calculation of reflectivity

The reflectivity is calculated after first finding $\epsilon_1(\omega)$ and $\epsilon_2(\omega)$, the real and imaginary parts of the dielectric function, respectively. The interband ϵ_2 is calculated from the band structure using

$$\epsilon_2^{\text{band}}(\omega) = \frac{e^2}{3\pi m^2 \omega^2} \sum_{c,v} \int \delta(E_c(\vec{k}) - E_v(\vec{k}) - \hbar\omega) \times \langle \Psi_c | \vec{p} | \Psi_v \rangle|^2 d^3k, \quad (6)$$

where c and v are the conduction- and valence-band indices. This expression is similar to that used by Brust,¹⁶ except that here Ψ_c and Ψ_v are the pseudopotential wave functions, not the actual wave functions which are orthogonalized to the core states. The integration over \vec{k} space is performed by the method described by Saslow *et al.*¹⁷ To obtain the total ϵ_2 , the interband contribution is added to the free-electron contribution given in the Drude-Zener theory¹⁸ by

$$\epsilon_2^{\text{free}}(\omega) = \omega_p^2 \tau / \omega (1 + \omega^2 \tau^2), \quad (7)$$

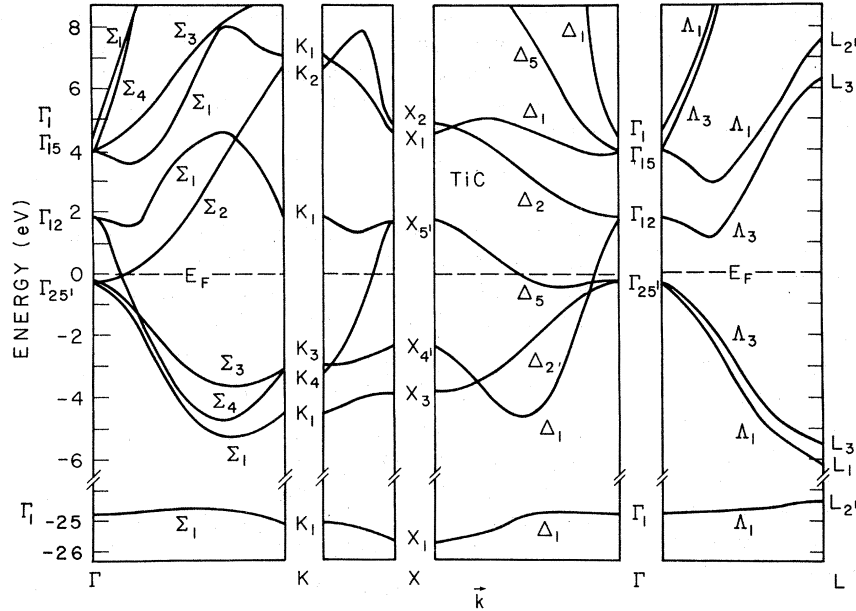


FIG. 2. Band structure of TiC.

where $\omega_p = (4\pi ne^2/m^*)^{1/2}$ is the plasma frequency,¹⁹ and $\tau = m^*\sigma/ne^2$ is the relaxation time. In these expressions, m^* is the effective mass, n is the effective concentration of free electrons, and σ is the experimentally determined value of the electrical conductivity. In a previous EPM calculation on palladium,²⁰ n was estimated from the volume enclosed by the Fermi surface centered at Γ_1 and m^* was roughly estimated by fitting a polynomial in $|\vec{k}|$ to the band energies at the Fermi surface: The curvature thus obtained was used to calculate $m^* = \hbar^2/(d^2E/dk^2)$. Unfortunately, the Fermi surface in the present case is quite complicated, so a reasonable estimation of m^* and n is very difficult; we shall resort to a parametrization. It is easy to show that ϵ_2^{free} , for fixed values of ω and σ , depends only on the parameter $\gamma \equiv m^*/n$ according to

$$\epsilon_2^{\text{free}}(\omega) = \frac{4\pi\sigma}{\omega(1 + \omega^2\gamma^2\sigma^2e^{-4})}. \quad (8)$$

Thus, the effective concentration and mass need not both be treated as empirical parameters—it is only the single parameter γ which, along with the pseudopotential parameters, is to be adjusted until satisfactory agreement with the reflectivity is obtained. The use of the single completely free parameter γ is more than justified when we consider the alternative: using, instead, two rather roughly estimated quantities, m^* and n .

With the above total $\epsilon_2(\omega)$, the Kramers-Kronig transformation²¹ is used to find the real part of the dielectric function, $\epsilon_1(\omega)$. Following Walter and Cohen,²² an analytic tail replacing the calculated $\epsilon_2(\omega)$ at high frequencies (~ 20 eV) is used in the transformation. Finally, the resulting $\epsilon_1(\omega)$ is used

with $\epsilon_2(\omega)$ to calculate the reflectivity.

IV. RESULTS: TiC

We shall first contrast our TiC band-structure results with those of others. The present experimental data are then compared to a previous reflectivity spectrum, and, finally, the present theoretical and experimental results are compared.

A. Comparison of TiC band structures

Our calculated electronic band structure along the various symmetry lines is given in Fig. 2 and the corresponding pseudopotential parameters are found in Table I: Listed are the two antisymmetric form factors, the three symmetric form factors, and the nonlocal parameters.

It is important to note the similarities and striking dissimilarities between the present band structure and the results of others.^{2,6,8,9} In the comparisons below (see also Table II) we shall pay special attention to differences in band ordering. While several investigators have reached conflicting conclusions regarding the direction of charge transfer and other bonding properties of TiC, we shall postpone a definitive final judgement on these matters until we have calculated the charge distribution for presentation in a future paper. We should preface our comments below with a few remarks regarding the energies of our 2s states. These states are very low compared to the other results mentioned below because a strong attractive antisymmetric potential $V^A(3)$ was needed to fit the energies of transitions involving p -like states; a much weaker potential would be necessary to adequately describe the 2s states. However, for the range of

TABLE I. Pseudopotential parameters for the band structure of TiC.

Parameters for local pseudopotential	Parameters for nonlocal d pseudopotential
$V^A(\vec{G} = 3(2\pi/a)^2) = 0.3642 \text{ Ry}$	$R_d = 1.1885 \text{ \AA}$
$V^A(11) = -0.0300$	$A_d = -4.3944 \text{ Ry}$
$V^S(4) = -0.1462$	$\kappa = 1.730(2\pi/a)^2$
$V^S(8) = -0.1100$	$\alpha = 0.210 \text{ \AA}^{-1}$
$V^S(12) = -0.0851$	

^aLattice constant $a = 4.326 \text{ \AA}$.

photon energy considered ($1.0 \leq \hbar\omega \leq 8.0 \text{ eV}$), these states, even if treated properly, would still be expected to lie too low to be of any consequence. Listed below are the relevant results of several investigators:

(i) Ern and Switendick⁹ calculated the band structure of TiC by the augmented-plane-wave (APW) method, using starting potentials derived from neutral atomic carbon ($2s)^2(2p)^2$, and titanium ($3d)^2(4s)^2$, in the respective spheres of their muffin-tin potentials. Their calculated band structure displays features which are very similar to ours—especially regarding the ordering of the bands. Except for the reversal of the order of their hybridized dp ($\Gamma_{15} - \Delta_5 - X_5'$) and hybridized sp ($\Gamma_{15} - \Delta_1 - X_1$) conduction bands, both the character and the ordering of their bands along Δ are the same as in the present work, and, in both cases, the bands cut by the Fermi surface are of hybridized dp character. Transitions between these two bands (4, 5) play the most important roles in our reflectivity calculations. The most significant differences between our results and theirs are that the energy gap $\Gamma_{25'} - \Gamma_{15}$ ($3d - 2p$) in their work (1.73 eV) is almost 2.5 eV lower than ours (4.21 eV), their titanium $4s(\Gamma_1)$ states are 5 eV higher, and their bands near the Fermi surface are flatter.

(ii) Conklin and Silversmith's self-consistent APW calculation⁹ confirmed, in general, the work of Ern and Switendick, the two main differences being that first, the pure d ($\Gamma_{25'} - \Delta_3 - X_3$) band of Conklin and Silversmith appears both above and below the Fermi surface, whereas this band in Ern and Switendick's work is entirely below the Fermi surface, just as in the present case; second, their $\Gamma_{15}(2p)$ state is very low—3.3 eV lower than ours, relative to $\Gamma_{25'}$.

(iii) In a tight-binding calculation, Bilz² determined the position of the carbon $2p$ states by averaging the one-electron energies of atomic carbon, nitrogen, and oxygen, in an effort to obtain a single band structure which might be conveniently applicable to TiC, TiN, and TiO. His p states associated with Γ_{15} are very low, lower than the Γ_{15} states of all the results mentioned above. Indeed, in his work Γ_{15} is 2.5 eV below $\Gamma_{25'}$. Such a result implies considerably less hybridization between the $3d$ and $2p$ states than has been found in other work.

(iv) Lye and Logothetis⁶ made a semiempirical tight-binding calculation of the band structure of TiC, using the two-center formalism of Slater and Koster.²³ A remarkable feature of their results is the very low placement of the titanium $4s$ states—at Γ they are more than 7 eV below the $3d$ ($\Gamma_{25'}$) states. Their $4s$ states are almost 12 eV lower (at Γ) than ours, and nearly 17 eV lower than Ern and Switendick's (Bilz and Conklin and Silversmith did not report the energies of the $4s$ states). In addition, their $2p$ states are the highest, relative to $\Gamma_{25'}$, of all the results reported above. Their theory, though, agrees with ours, and with the others regarding the character (hybridized dp) of the states at the Fermi level.

B. Reflectivity: TiC

Our experimental reflectivity curve is compared to the data of Lye and Logothetis⁶ in Fig. 3. Below

TABLE II. Comparison of important energy gaps obtained from the present EPM and past APW and tight-binding calculations.

Energy gaps symmetry	Bilz tight-binding (eV)	Ern and Switendick APW (eV)	Lye and Logothetis tight-binding (eV)	Conklin and Silversmith self-consistent APW (eV)	Present EPM (eV)
$\Gamma_{25'} \rightarrow \Gamma_{15}$	-2.50	1.73	5.65	0.89	4.21
$\Gamma_{12} \rightarrow \Gamma_{15}$	-3.20	0.76	3.50	-0.03	2.11
$\Gamma_{25'} \rightarrow \Gamma_1$		9.48	-7.15		4.50
$X_4' \rightarrow \Gamma_{12}$	-1.45	4.04	3.30	4.79	4.19
$\Gamma_{25'} \rightarrow X_5'$	-0.90	0.28	3.05	-0.62	1.94
$X_3 \rightarrow \Gamma_{25'}$	0.80	1.91	2.55	2.00	3.58
$\Gamma_{12} \rightarrow X_2$	0.80	0.75	1.70	0.80	3.01
$\Gamma_{25'} \rightarrow \Gamma_{12}$	0.70	0.97	2.15	0.92	2.10
$\Gamma_{15} \rightarrow L_{2'}$	2.90	1.21	-4.50	2.02	3.69

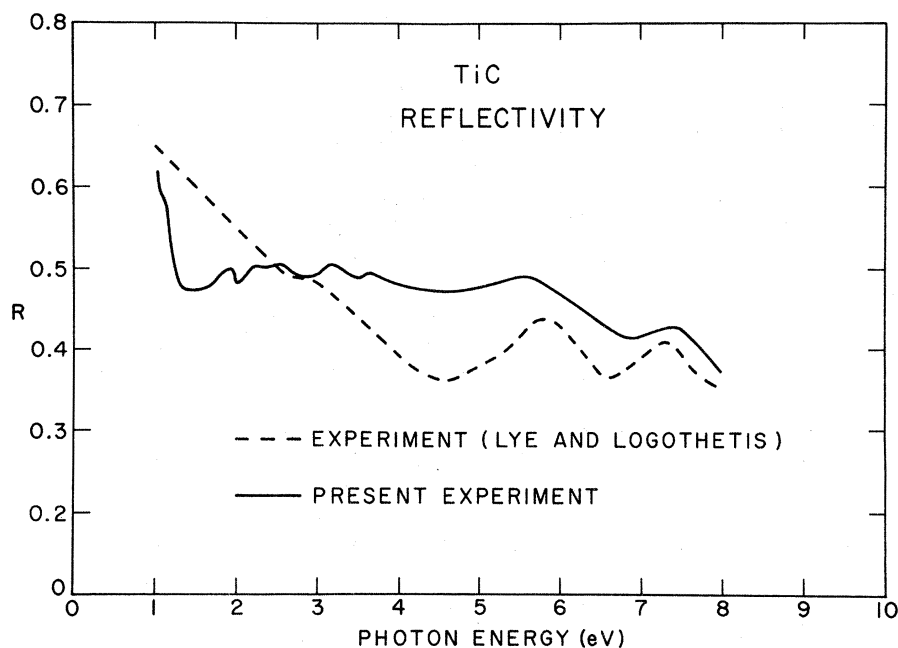


FIG. 3. Comparison of present reflectivity curve for TiC with the data of Lye and Logothetis.

2.5 eV, our reflectivity curve is about 5% (absolute) lower, on the average, than theirs, and about 5% higher above 2.5 eV. Because of imperfections on the sample surface, they had to correct for the resulting losses by comparing the reflected intensities from aluminum films evaporated on the sample surface and on a flat glass surface, respectively. However, we believe that the practical limitations imposed by this method on the reproducibility of the sample surface would limit the accuracy of determining the absolute value of the reflectivity. Furthermore, it would also limit the determination of the effect of wavelength-dependent scattering from the actual sample surface imperfections.

Our measured curve about 4 eV shows the same peaks present in their work: Our peaks at 5.6 and 7.2 eV correspond to theirs at 5.5 and 7.2 eV. However, below 4 eV our spectrum shows more structure—because of the better resolution of our apparatus—and tends to be flatter down to 1.4 eV where it starts to rise abruptly. The larger reflectivity below 3 eV in their data is not surprising when we consider that the lower stoichiometry of their sample ($\text{TiC}_{0.794}$), compared to ours ($\text{TiC}_{0.999}$), should mean a larger free-electron concentration, with correspondingly stronger free-electron behavior. This should lead to a higher plasma frequency and hence a more abrupt fall at higher energy than in our case. However, since the scattering losses due to surface irregularities mentioned in their work are expected to increase with decreasing wavelength (increasing energy) of incident light, they observe a gradually decreasing curve instead of an abrupt fall.

We have calculated the total density of states for TiC, using a linear interpolation of about 10 000 randomly generated points in a mesh of 46 points for each of the ten bands shown in Fig. 2. The resolution of the density of states is 0.1 eV. The value of the Fermi energy was determined to be $E_F = 7.3$ eV, the upper limit on a density-of-states summation to a total of eight electrons. In Fig. 4 we show the histogram density of states for energies within ± 5 eV of E_F . Note that the Fermi energy occurs very near the minimum in the density of states; similar results have been obtained by others.^{6,8,9}

In Fig. 5, separate curves of the free-electron and interband ϵ_2 for TiC are given; our interband curve was smoothed from our histogram plot (not shown) by averaging the values in three adjoining intervals. The free-electron curve was obtained from Eq. (8) using the value of the electrical conductivity reported by Samsonov²⁴ ($\sigma = 1.96 \times 10^{15}$ esu) and the value of the free-electron parameter ($\gamma = 1.19 \times 10^{-49}$ g cm³) giving the best fit to the reflectivity data. We can show that this value of γ is realistic. If, for example, the effective mass of the electron were simply the free-electron mass m_0 , then our value of γ would correspond to 0.155 free electrons per molecule of TiC, which is, incidentally, comparable to the values obtained in Hall-coefficient measurements¹ of the number of conduction electrons per molecule of TiC at room temperature (recall that our measurements were also made at room temperature): Reported values range from 0.08 to 0.18 electrons per molecule. For completeness, we may state that the calculated

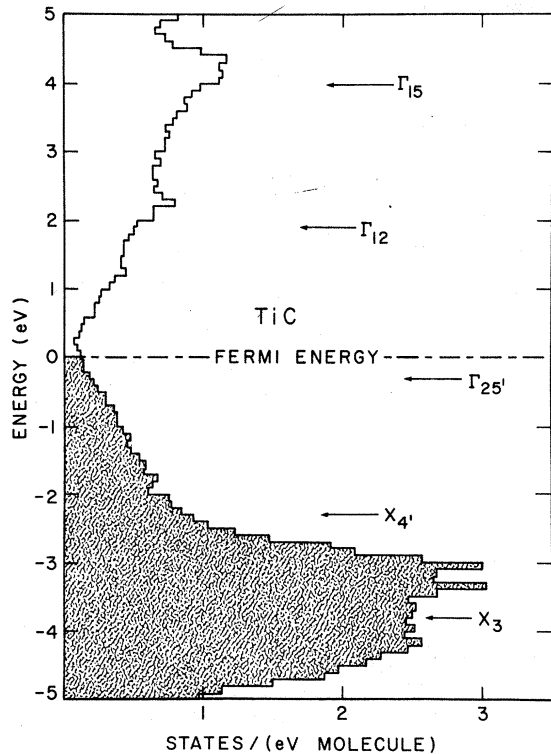


FIG. 4. Histogram density of states for TiC. Filled region is shaded.

value of the free-electron plasma energy is

$$\hbar\omega_p = (4\pi\hbar^2 e^2 \gamma^{-1})^{1/2} = 3.23 \text{ eV},$$

and the relaxation time

$$\tau = \gamma\sigma e^{-2} = 9.31 \times 10^{-15} \text{ sec}$$

is comparable to values found in copper and silver ($\approx 10^{-14}$ sec).

Our calculated reflectivity is compared to our measured curve in Fig. 6. While there is a large difference in magnitude, the general shape of the theoretical reflectivity agrees with the experiment and there is a one-to-one correspondence to the structures in the data for the entire range of photon energy, with agreement to the order of 0.2 eV (the corresponding structures in the experiment and theory are numbered). The many extra smaller structures in the theory which do not find correspondence to the data (especially above 4 eV) could be due, in part, to the fact that our Hamiltonian was diagonalized on a relatively coarse mesh (46 points) in the irreducible zone, though this assumption, if valid, could call into question some of the weakest structures below 4 eV. A more satisfactory explanation is that accounting for thermal broadening would no doubt smear out some of the neighboring peaks in the calculated spectra, affording better agreement with the room-temperature measurement. Experiment and theory show a very pronounced dissimilarity between 2.2 and 3.2 eV; the shape of the broad structure in the theory bears little resemblance to the structure (numbered 3, 4, and 5) in the data. In the theory, the strong transition at 2.6 eV almost completely masks the weaker shoulders appearing on either side of it. Many attempts were made to remedy this condition; unfortunately, since these structures are not associated with critical points, but with large volumes in the zone, better agreement in this region could not be obtained without completely destroying the good agreement in other parts of the spectrum.

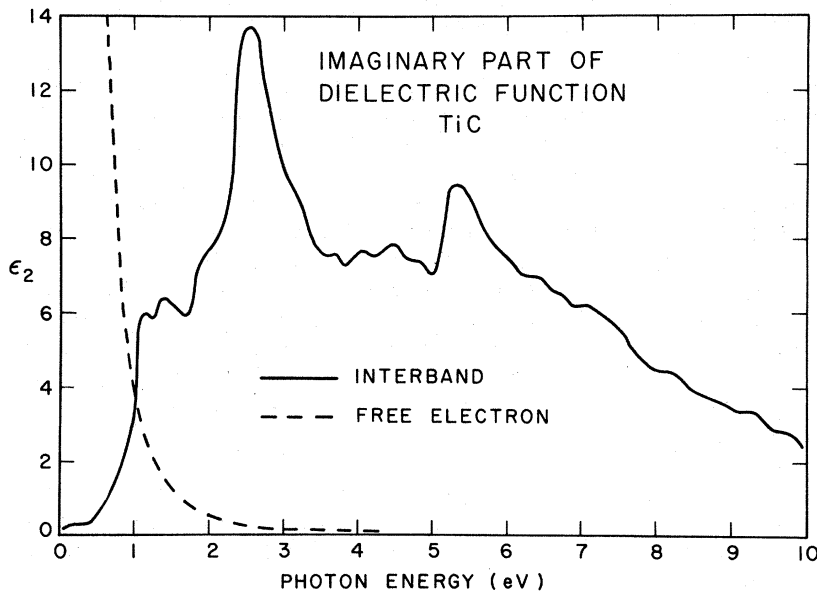


FIG. 5. Interband and free-electron ϵ_2 calculated for TiC.

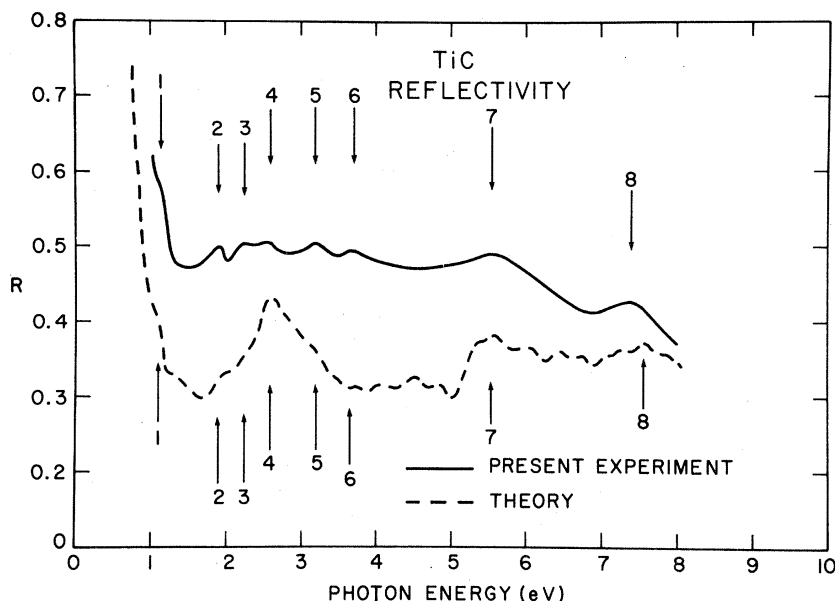


FIG. 6. Comparison of theoretical and experimental reflectivity spectra for TiC. The structures in the data which find correspondence to the theory are numbered for easy comparison.

As mentioned earlier, another point of disagreement is the severe difference of magnitude over the entire energy range—an average *absolute* difference of about 10% (as much as 20% between 4 and 5 eV). We have attempted to attribute this difference in magnitude to a dipole-matrix-element effect: if the actual wavefunctions (which are orthogonalized to the core states) are used instead of the smooth pseudopotential wave functions, one expects, in general, an increase in the magnitude of these matrix elements, with a corresponding increase in the reflectivity. However, we have tested this hypothesis for two of the most important transitions [3-5 near $\Sigma(\frac{1}{8}, \frac{1}{8}, 0)$, and 4-5 near a point just above the center of Δ] and found that the *relative* strength of the 4-5 transition increases by only about 10%, while the 3-5 decreases by 10%. Thus, if we use the actual wave functions, we can expect only a very small improvement. This slight improvement is reasonable in light of the fact that these transitions (and almost all of the other important transitions) involve hybridized dp states which one expects would lie in the region between the atoms, and therefore any improvement associated with core orthogonalization should be small. Further comment on the difference in magnitude between the theoretical and experimental reflectivities shall be deferred until we discuss our conclusions in Sec. VI.

The origins of the important peaks appearing in the reflectivity of TiC are summarized in Table III. It is interesting to note that most of the structures are not closely associated with critical points; we find that the 3-5 and 4-5 transitions on or near the base ($\Gamma K W X$) of the zone are the major components of the structures; the 4-5 transition is the

largest component for all but the shoulder at 1.1 eV, where 3-5 is the most prominent. For the peak at 7.5 eV, the 3-5 and 4-5 transitions are of about equal strength.

On the basis of their band structure, Lye and Logothetis determined that $4s-2p$ transitions between occupied $4s$ -like states and vacant $2p$ -like states near $\vec{k} = (\frac{1}{2}, \frac{3}{16}, \frac{3}{16})\pi/a$ are responsible for the structure at 6 eV in their optical-conductivity spectrum (not shown), which they obtained from a dispersion analysis of their reflectivity. The corresponding peak in our data (number 7, at 5.6 eV) arises from transitions from large regions of the zone between the fourth and fifth (hybridized dp) bands. They furthermore maintain that their peak at 7.2 eV is due to transitions near the square face of the zone from occupied p -like states (X'_4) to vacant s -like states (X_1), whereas our calculation indicates that the 7.2-eV peak is due to 3-5 and 4-5 transitions (the 3-5 is the stronger) involving the hybridized dp states from regions near the base of the zone.

While there is a large difference in the magnitudes of our measured and calculated reflectivity spectra for TiC, we nevertheless find one-to-one correspondence for six out of seven structures in the theory below 4 eV (the single noncorresponding low-energy structure in the theory is the shoulder at 1.5 eV), in addition to finding general agreement of shape over the entire energy range.

V. RESULTS: ZrC

In this section we shall present the band structure and experimental and theoretical reflectivities for ZrC, and the results shall be compared with TiC.

TABLE III. Identification of structures in the reflectivity of TiC.

Structure No.	Transitions	Energy (eV) theory	Energy (eV) experiment	Symmetry (strongest component)
1	2-5(weak), 3-5(strong), 4-5	1.1	1.1	(3-5): near Γ
2	2-5(weak), 3-5, 4-5(strong)	1.9	1.9	(4-5): contour parallel to Δ from near Γ to near X on base ($\Gamma K W X$) of zone.
3	3-5, 4-5(strong)	2.2	2.2	(4-5): same as 1.9-eV contour but slightly displaced above the base
4	3-5, 3, 4, 5-6(weak), 4-5(strong)	2.6	2.6	(4-5): contour from $\Sigma(1/3, 1/3, 0)$ to X on the base of the zone
5	3-5, 4-5-6(weak), 4-5(strong)	3.2	3.2	(4-5): contour parallel to Δ along central region of the base
6	3-5, 6, 7, 4-5(strong), 4-6	3.7	3.7	(4-5): contour parallel to Δ above central region of the base
7	3-5, 3-6, 7, 8(weak), 2-5(strong), 4-5(strong)	5.6	5.6	(4-5): region on and above the central area of base
8	2-5, 3, 4-6, 7, 3-5(strong), 4-5(strong)	7.5	7.2	(3-5): contour from $\Sigma(1/2, 1/2, 0)$ to W , on and above the base; (4-5) contour same as the (3-5)

A. Band structures of ZrC

Satisfactory results for ZrC were obtained on the first try by slightly adjusting form factors scaled from TiC; no form factor was changed by more than 0.02 Ry. We should emphasize that the nonlocal parameters α and κ for ZrC were not fitted to the data, as they were for TiC. We have assumed that the \vec{k} -dependent damping factor [see Eq. (5)] is the same for both compounds; thus, the value of α is adjusted from its value for TiC to compensate for both the different lattice constants and Fermi momenta. The parameter κ is in units of $2\pi/a$, so no change is necessary. The band structure of ZrC is given in Fig. 7, and the corresponding pseudopotential parameters appear in Table IV. Except for the lower $2p$ (Γ_{15}) state in ZrC, and the crossing of the lower two conduction bands along for ZrC, there is comparatively little difference between the band structures of ZrC and TiC, as might be expected: Zirconium is just below titanium in Group IVB of the Periodic Table. The main differences between the two compounds are the larger lattice constant of ZrC ($a = 4.683 \text{ \AA}$) compared to TiC ($a = 4.326 \text{ \AA}$) and the larger core in Zr. There is no way to scale from the TiC calculation new values for the depth and width of the nonlocal d potential, and they must be treated as

parameters to be adjusted. One expects, however, that the difference in core sizes should be reflected in a wider well for ZrC; we have found that the best fit to the ZrC data is obtained by using $R_d = 1.3497 \text{ \AA}$, compared to $R_d = 1.1885 \text{ \AA}$ for TiC. Furthermore, since the core in Zr includes $3d$ states, we should expect the attractive nonlocal d potential to be weaker; the best fit was obtained with $A_d = -3.1077 \text{ Ry}$ for ZrC, compared to $A_d = -4.3944 \text{ Ry}$ for TiC.

B. Reflectivity: ZrC

In Fig. 10 the solid curve is our measured reflectivity spectrum for ZrC. In comparison with

TABLE IV. Pseudopotential parameters for the band structure of ZrC.

Parameters for local pseudopotential	Parameters for nonlocal d pseudopotential
$V^A [\vec{G} = 3(2\pi/a)^2] = 0.3122 \text{ Ry}$	$R_d = 1.3497 \text{ \AA}$
$V^A(11) = -0.0300$	$A_d = -3.1077 \text{ Ry}$
$V^S(4) = -0.0987$	$\kappa = 1.73 (2\pi/a)^2$
$V^S(8) = -0.0850$	$\alpha = 0.174 \text{ \AA}^{-1}$
$V^S(12) = -0.0558$	

^aLattice constant $a = 4.683 \text{ \AA}$.

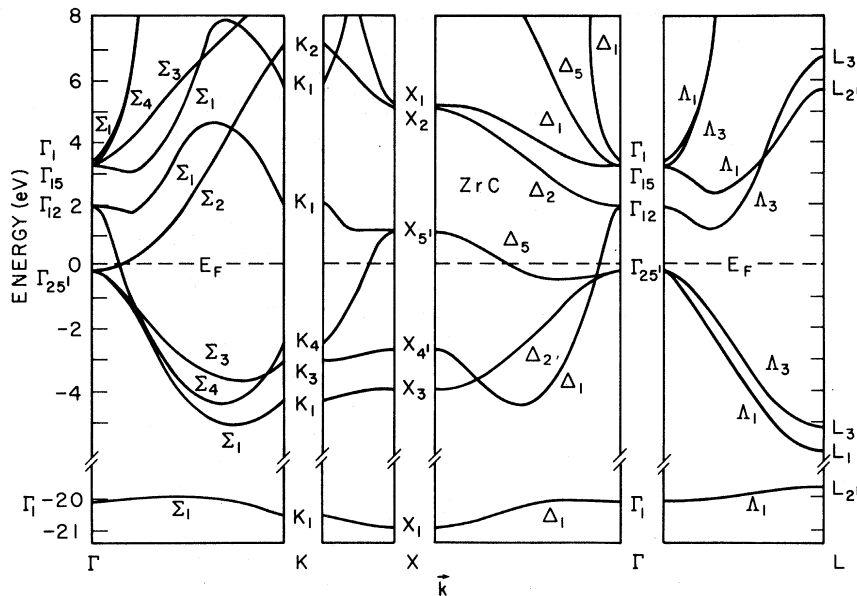


FIG. 7. Band structure for ZrC.

our experimental reflectivity of TiC in Fig. 3, we note that the general shapes are similar, and each has roughly the same structures. However, the measured magnitude above 1 eV in TiC is significantly greater than for ZrC; above 1.2 eV, the reflectivity for TiC is 8% higher (absolute), on the average. Since the stoichiometries of the crystals are about the same, and since the samples were prepared in the same manner, one would expect that both compounds would have reflectivity spectra of about the same magnitude, especially since the valence electrons of each compound come from

similar electronic configurations. However, this is not the case. As noted by Nilsson,²⁵ optical-absorption results are critically dependent on the degree of surface smoothness. Thus, the differences observed here are not surprising because the extreme hardness of both samples made it almost impossible to obtain the same surface characteristics for each.

The interband and free-electron contributions to ϵ_2 are shown in Fig. 8. The calculated free-electron contribution is slightly greater here than was the case for TiC. The parameter $\gamma = m^*/n = 1.02$

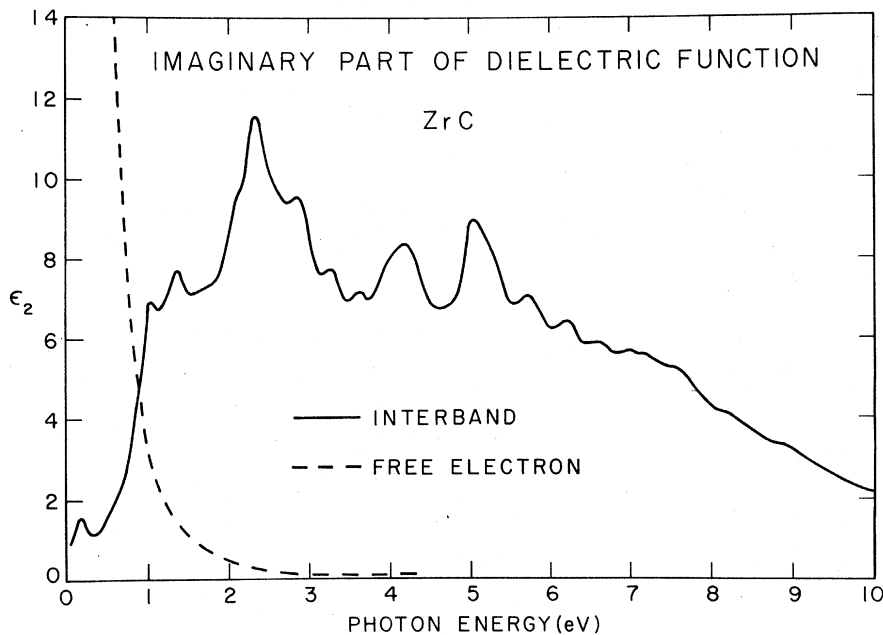


FIG. 8. Interband and free-electron ϵ_2 calculated for ZrC.

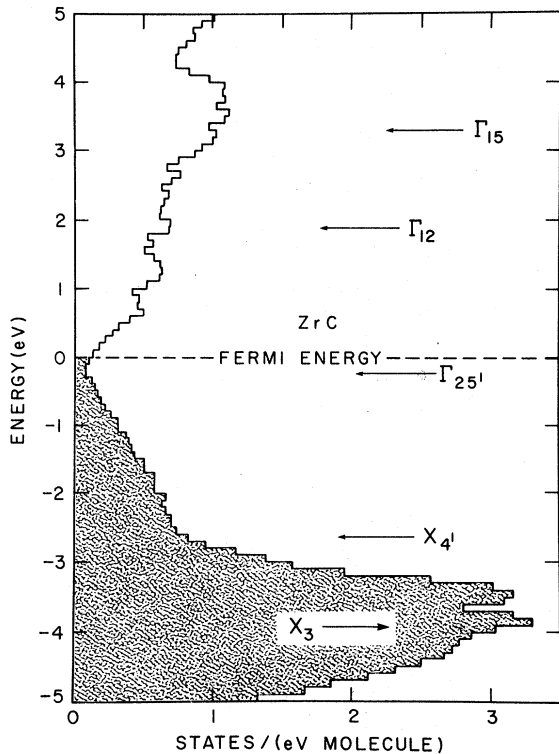


FIG. 9. Histogram density of states for ZrC. Filled region is shaded.

$\times 10^{-49}$ g cm³ for ZrC, compared to $\gamma = 1.19 \times 10^{-49}$ g cm³ for TiC. We may put this difference in perspective: If we could assume that the lower density of states near the Fermi energy (the Fermi energy is taken to be the zero of energy) in

the ZrC calculation ($n = 0.091$ states/molecule—see Fig. 9) compared to TiC ($n = 0.121$ states/molecule) implies a correspondingly lower free-electron concentration in the sample, then the smaller value of γ needed for ZrC could only be explained in terms of a smaller actual effective mass in the sample.

The experimental value of the conductivity for ZrC is $\sigma = 2.00 \times 10^{15}$ esu.²⁴ Corresponding to this value of σ and the value of γ mentioned above, the free-electron plasma energy is found to be 3.10 eV, slightly smaller than that obtained for TiC (3.23 eV), and the relaxation time is 1.01×10^{-14} sec ($\tau = 9.3 \times 10^{-15}$ sec for TiC).

The calculated reflectivity of ZrC is compared with the present experimental data in Fig. 10. The general shape and magnitude of the calculated spectra agrees quite well with the measured curve, though there is a (10–20)% difference in magnitude between 1 and 2 eV. The general agreement of magnitude is significantly better than was found for TiC—especially in the region above 2.3 eV: For ZrC the agreement is within 6%, whereas the difference between data and theory for TiC is (5–20)%. In addition, nine of eleven discernable structures in the data for ZrC find good correspondence to structures in the theory—the agreement is within 0.2 eV for all but the peak at 7.7 eV in the theory (the experimental value is 7.2 eV). The origins of the (numbered) structures in the measured spectra are noted in Table V. As expected, the structures in the data of ZrC have essentially the same origins as the structures in TiC, and except for the structure at 5.2 eV in ZrC (where the 2-5 is dominant), 4-5 transitions associated with regions close to the base of the zone are the major constituents of the

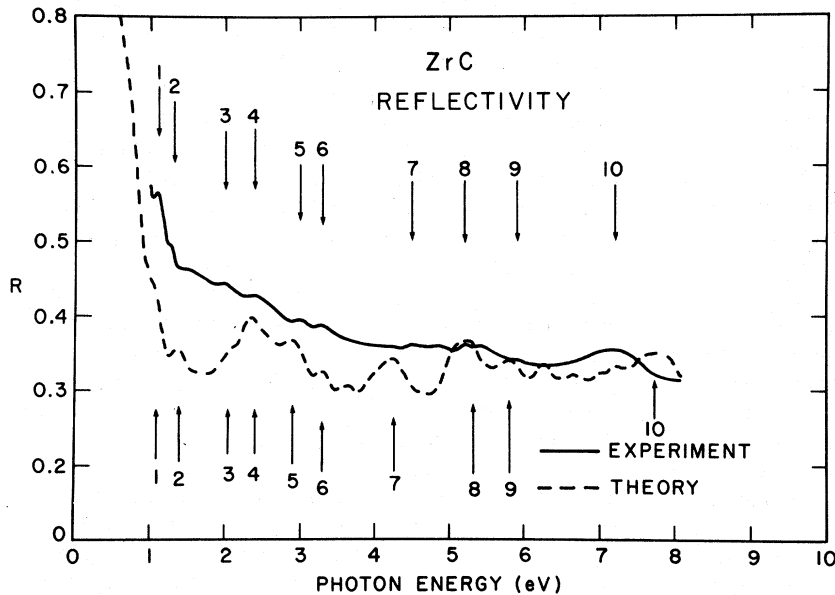


FIG. 10. Comparison of theoretical and experimental reflectivity spectra for ZrC. The structures in the data which find correspondence to the theory are numbered for easy comparison.

TABLE V. Identification of structure in reflectivity of ZrC.

Structure No.	Transitions	Energy (eV) theory	Energy (eV) experiment	Symmetry (strongest component)
1	2-5(weak), 3-5 4-5(strong)	1.1	1.1	(4-5): contour from near Γ to near X on the base ($\Gamma K W X$) of the zone
2	2,3-5, 4-5(strong)	1.3	1.3	(4-5): contour neighboring the 1.1-eV contour
3	2-5(weak), 3-5, 4-5(strong)	2.0	2.0	(5-4): contour on the base through center from near Γ to near X
4	2-5(weak), 4-6 (weak), 4-5 (strong)	2.4	2.4	(4-5): contour displaced slightly from the 2.0-eV contour toward central area of base
5	3,5-6(weak), 3-5, 4-5(strong), 4-6 (weak)	2.9	3.0	(4-5): central contour on the base from near $\Sigma(1/3, 1/3, 0)$ to near W
6	3-4(weak), 3-5, 4-5(strong), 4-6	3.3	3.3	(4-5): contour displaced slightly from the 2.9-eV contour
7	2-5(weak), 3-5, 3-6(weak), 3-7, 4-5(strong), 4-6, 7	4.2	4.5	(4-5): contour on and above the base, from $\Sigma(1/3, 1/3, 0)$ to near W
8	2-5(strong), 3-5, 3-6(weak), 4-5, 6, 7	5.1	5.2	(2-5): contour from near $\Sigma(1/3, 1/3, 0)$ to near X , on and just above the base
9	2-5, 3-5, 3-6, 7 (weak), 4-5(strong), 4-6, 7	5.8	5.9	(4-5): contour on the base from $\Sigma(1/2, 1/2, 0)$ to W
10	2-5, 7(weak), 3-5, 3-6, 7(weak), 4-5 (strong), 4-6, 7	7.7	7.2	(4-5): contour just above the base from $\Sigma(1/2, 1/2, 0)$ to near W

structures.

VI. SUMMARY AND CONCLUSIONS

We have measured the optical reflectivities for TiC and ZrC and have found general shape and structure agreement between the two sets of data. The significant difference in magnitude between the two measured reflectivity curves probably arises from differences in the smoothness of the two samples which could not be remedied because of the extreme hardness of these carbides. We have also calculated the band structures and reflectivities for these compounds using a modified empirical pseudopotential method. The over-all agreement between data and theory for TiC is satisfactory: rather disappointing agreement in the general shape of the spectra between 2 and 4 eV, and everywhere a large difference in magnitude, but good correspondence of structures over the entire energy range. Since the magnitudes of the calculated spectra for both TiC and ZrC are about the same, as expected, we

cannot at once attribute the difference in magnitude between theory and data for TiC to inadequacies of the theory, though this is a possibility and is now under investigation. As already mentioned, the more likely reason for the relatively poor agreement of magnitude is the difficulty in preparing a near-perfect sample surface. The results for ZrC, both theory and data, show satisfactory agreement regarding shape, magnitude, and structure position.

Our band structure for TiC generally agrees with the results of Ern and Switendick, and with Conklin and Silversmith regarding band ordering, though the $\Gamma_{25'} - \Gamma_{15}$ energy gaps in both of these works are significantly smaller than we have found. A more startling contrast is found in comparison with the tight-binding results of Lye and Logothetis where we find severe disagreement with their placement of the 4s states; theirs are completely occupied, and ours are empty. However, our results are in agreement with all of the previous results on one point: the states at the Fermi surface arise from a

hybridization of the $3d$ and $2p$ orbitals.

The present calculations adequately explain the optical properties of TiC and ZrC, and the agreement in position of the structures to the order of 0.2 eV indicates that both band structures are accurate to the same order. We have not speculated on the extent of charge transfer between carbon and titanium in TiC, as has been done by other investigators, since the wave functions obtained in the

present calculation of the band structure of TiC will be used soon in a calculation of the charge distribution.

ACKNOWLEDGMENTS

The authors wish to thank Dennis L. Rogers for many useful discussions and a critical reading of the manuscript. Thanks are also due T. Hillyer for assistance with the measurements.

[†]Work supported in part by the U. S. Air Force Office of Scientific Research (AFSC) under Grant No AFOSR-72-2353.

*On leave from Department of Applied Mathematics and Physics, Faculty of Engineering, Cairo University.

¹L. E. Toth, *Transition Metal Carbides and Nitrides* (Academic, New York, 1971), and references therein.

²H. Bilz, *Z. Phys.* **153**, 338 (1958).

³S. P. Denker, *J. Phys. Chem. Solids* **25**, 1397 (1964).

⁴S. P. Denker, *J. Less-Common Metals* **14**, 1 (1968).

⁵R. G. Lye, RIAS Tech. Rep. No. 66, 1966 (unpublished).

⁶R. G. Lye and E. M. Logothetis, *Phys. Rev.* **147**, 622 (1966). They made reflectivity measurements from 0.5 to 21 eV on TiC_x specimens; they measured the low-energy region (0.5–5.8 eV) on TiC_{0.784} and assumed the results applied to all other samples, even to their sample of highest stoichiometry, TiC_{0.951}.

⁷R. G. Lye, in *Atomic and Electronic Structure of Metals* (American Society of Metals, Metals Park, Ohio, 1967), p. 99.

⁸V. Ern and A. C. Switendick, *Phys. Rev.* **137**, A1927 (1965).

⁹J. B. Conklin Jr. and D. J. Silversmith, *Int. J. Quantum Chem.* **2S**, 243 (1968).

¹⁰M. L. Cohen and V. Heine, in *Solid State Physics*, edited by Seitz and Turnbull (Academic, New York, 1970), Vol. 24, p. 37.

¹¹C. Y. Fong and M. L. Cohen, *Phys. Rev. Lett.* **24**, 306

(1970).

¹²C. Y. Fong and M. L. Cohen, *Phys. Rev. B* **6**, 3633 (1972).

¹³G. B. Irani, T. Huen, and F. Wooten, *Appl. Opt.* **10**, 552 (1971).

¹⁴G. B. Irani, T. Huen, and F. Wooten, *Phys. Rev. B* **3**, 2385 (1971).

¹⁵D. J. Chadi and M. L. Cohen, *Phys. Rev. B* **10**, 496 (1974).

¹⁶D. Brust, *Phys. Rev.* **134**, A 1337 (1964).

¹⁷W. Saslow, T. K. Bergstresser, C. Y. Fong, M. L. Cohen, and D. Brust, *Solid State Commun.* **5**, 667 (1967).

¹⁸J. M. Ziman, *Principles of the Theory of Solids* (Cambridge U. P. Cambridge, 1964), p. 239.

¹⁹Reference 18, p. 225.

²⁰C. Y. Fong, *J. Phys. F*: **4**, 775 (1974).

²¹F. Wooten, *Optical Properties of Solids* (Academic, New York, 1972), p. 179.

²²J. P. Walter and M. L. Cohen, *Phys. Rev.* **183**, 763 (1969).

²³J. C. Slater and G. F. Koster, *Phys. Rev.* **94**, 1498 (1954).

²⁴G. V. Samsonov, *High-Temperature Materials, Properties Index* (Plenum, New York, 1964).

²⁵P. O. Nilsson, in *Solid State Physics*, edited by Seitz and Turnbull (Academic, New York, 1974), Vol. 29, p. 173.